Analysis of Dihydrogen Bonding in Ammonium Borohydride

THE JOURNAL OF PHYSICAL CHEMISTRY C

Article

Cite This: J. Phys. Chem. C 2019, 123, 28631−28639

pubs.acs.org/JPCC

Analysis of Dihydrogen Bonding in Ammonium Borohydride

Stanislav Filippov,[†,‡] Jakob B. Grinderslev,[§] Mikael S. Andersson,[∥] Jeff Armstrong,[⊥] Maths Karlsson,[∥] Torben R. Jensen,[§] Johan Klarbring,[†] Sergei I. Simak,[†] and Ulrich Häussermann*[,‡]

[†]Theoretical Physics Division, Department of Physics, Chemistry and Biology (IFM), Linköping University, SE-58183, Linköping, Sweden

[‡]Department of Materials and Environmental Chemistry, Stockholm University, SE-10691 Stockholm, Sweden

[§]Center for Materials Crystallography, Interdisciplinary Nanoscience Center (iNANO) and Department of Chemistry, Aarhus University, Langelandsgade 140, 8000 Aarhus C, Denmark

[∥]Department of Chemistry and Chemical Engineering, Chalmers University of Technology, SE-41296 Gothenburg, Sweden

[⊥]ISIS Facility, Rutherford Appleton Laboratory, Chilton, Didcot, Oxfordshire OX11 0QX, U.K.

ABSTRACT: The structural and vibrational properties of ammonium borohydride, NH_4BH_4, have been examined by first-principles density functional theory (DFT) calculations and inelastic neutron scattering (INS). The H disordered crystal structure of NH_4BH_4 is composed of the tetrahedral complex ions NH_4^+ and BH_4^-, which are arranged as in the fcc NaCl structure and linked by intermolecular dihydrogen bonding. Upon cooling, the INS spectra revealed a structural transition between 45 and 40 K. The reversible transition occurs upon heating between 46 and 49 K. In the low-temperature form reorientational dynamics are frozen. The libration modes for BH_4^- and NH_4^+ are near 300 and 200 cm^{-1}, respectively. Upon entering the fcc high-temperature form, NH_4^+ ions attain fast reorientational dynamics, as indicated in the disappearance of the NH_4^+ libration band, whereas BH_4^- ions become significantly mobile only at temperatures above 100 K. The vibrational behavior of BH_4^- ions in NH_4BH_4 compares well to the heavier alkali metal borohydrides, $NaBH_4$-$CsBH_4$. DFT calculations revealed a nondirectional nature of the dihydrogen bonding in NH_4BH_4, with only weak tendency for long-range order. Different rotational configurations of complex ions appear quasi-degenerate, which is reminiscent of glasses.

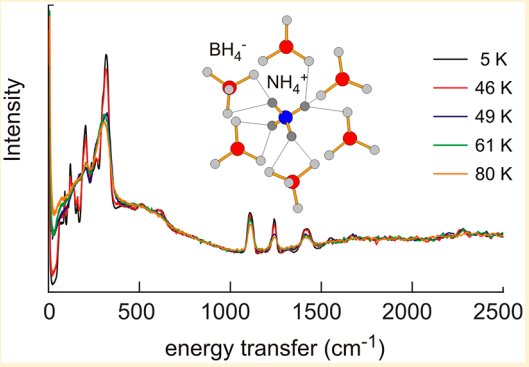

1. INTRODUCTION

Ammonium borohydride, NH_4BH_4, has one of the highest gravimetric and volumetric H densities among solid compounds (ρ_m = 24.5 wt %, ρ_V = 157.3 g H_2/L at room temperature) and is therefore an interesting hydrogen storage material.[1] Its synthesis was first reported in 1958 and employs a metathesis reaction between NH_4F and $NaBH_4$ in liquid ammonia.[2] The H disordered crystal structure of NH_4BH_4 is composed of the tetrahedral complex ions NH_4^+ and BH_4^-, which are arranged as in the fcc NaCl structure. The simultaneous presence of hydridic and protonic H gives rise to strong intermolecular bonding—dihydrogen bonding—while at the same time introducing an inherent instability toward H_2 release.[3] The decay of NH_4BH_4 proceeds over hours at room temperature, whereas below 240 K the material can be stored indefinitely.[2,3]

Dihydrogen bonding has been considered an unusual type of hydrogen bonding and attracted considerable attention since the mid-1990s for its significance to structural properties, reactivity, and selectivity of compounds in solution and solid state.[4,5] In this respect, NH_4BH_4 represents a special case because of the exceptional large number of hydridic-to-protonic contacts that can be realized between the cationic and anionic species. Yet, in contrast with ammonia borane, BH_3NH_3, there have been only few investigations into the nature of dihydrogen bonding and its consequences to structural and dynamic properties in NH_4BH_4. The average NaCl structure was established as late as in 2009.[3] Subsequently, models for the H disordered structure were reported from synchrotron and neutron powder diffraction data. The fcc phase appears to be stable down to 60 K. At lower temperatures, transitions to lower symmetry structures occur.[6,7]

Recent investigations by molecular dynamics (MD) calculations and solid state ^1H and ^2H NMR measurements revealed the presence of dynamic disorder, corresponding to very rapid reorientation of both ions, in the temperature range 100−250 K.[8] In particular, activation energies of around 11 kJ/mol were extracted from the temperature dependence of spin−lattice relaxation times. The data did not allow separation of the contributions to relaxation arising from each ion, and it was assumed that the individual activation energies are quite

Received: September 20, 2019
Revised: November 3, 2019
Published: November 4, 2019

similar. Also, NMR experiments and MD simulations gave consistent values for the correlation time at 300 K, which was found to be in the range 14−16 ps. Theoretical calculations of barriers for rotation, however, hinted that BH_4^- is slightly more hindered than NH_4^+.[8] NH_4BH_4 was further investigated at high-pressure conditions where it was found that the ambient pressure fcc phase initially transforms into a highly disordered intermediate structure which then, between 3.4 and 4.6 GPa, evolves into an orthorhombic, distorted CsCl structure. Interestingly, MD calculations revealed that NH_4BH_4 maintains a high degree of mobility when pressurized.[9]

The detailed mechanism of the dynamics of constituting ions in fcc NH_4BH_4 remains unknown. Furthermore, it is unclear whether the dynamics freezes out at lower temperatures, leading to ordering of the complex ions, which could explain the structural transitions observed in neutron diffraction experiments at temperatures below 60 K.[6,7] In this work we analyze the energetics of dihydrogen bonding by first-principles calculations and characterize the vibrational properties of NH_4BH_4 by using inelastic neutron scattering (INS). The intensity of the scattering is dependent on the amplitude of the vibration as well as the incoherent scatter cross section.[10] For hydrogen both quantities are large, and therefore INS spectroscopy is especially sensitive to the vibrations of hydrogen atoms. Thus, it is expected that INS can give insight into the dihydrogen bonding phenomenon of NH_4BH_4 as well as information about expected disorder−order structural transitions at low temperatures.

2. METHODS

2.1. Synthesis of $NH_4{}^{11}BH_4$. $Na^{11}BH_4$ and $NH_4{}^{11}BH_4$ were synthesized by following previously published procedures.[2,11] $Na^{11}BH_4$ was synthesized from NaH and $S(CH_3)_2{\cdot}{}^{11}BH_3$. First, NaH (dry, 95%, Sigma-Aldrich) was mechanochemically activated by ball milling using a Fritsch Pulverisette 6 planetary ball mill under inert conditions. Powdered NaH was loaded and sealed into an 80 mL tungsten carbide vial with tungsten carbide balls (5.5 g mass) in an argon-filled glovebox using a ball to powder weight ratio of 30:1. The powder was milled at 350 rpm 10 times for 10 min. Each interval was intervened by a 2 min break. The as-milled NaH was then mixed with $S(CH_3)_2{\cdot}{}^{11}BH_3$ (50% molar excess, 10 M, Katchem) and diluted to 5 M by using toluene (anhydrous, Sigma-Aldrich). The mixture was left stirring at T = 333 K (60 °C) for 1 week, resulting in $Na^{11}BH_4$. $NH_4{}^{11}BH_4$ was synthesized by stirring $Na^{11}BH_4$ with a 10% molar excess of NH_4F (≥99.99%, Sigma-Aldrich) in liquid NH_3 at T = 195 K (dry ice/ethanol). $NH_4{}^{11}BH_4$ is formed after ∼4 h. The bydroducts, NaF and unreacted NH_4F, were removed by filtration. Excess and coordinated NH_3 was removed under vacuum at T = 233 K to recover $NH_4{}^{11}BH_4$ as a white polycrystalline powder. The samples were stored in a glovebox freezer at T = 239 K (−34 °C).

2.2. Synchrotron Radiation Powder X-ray Diffraction. $NH_4{}^{11}BH_4$ was characterized by high-resolution synchrotron radiation powder X-ray diffraction (SR PXD). The powdered sample was packed in a borosilicate capillary (i.d. 0.5 mm) in an argon-filled glovebox ($p(O_2, H_2O)$ < 1 ppm), and samples were shipped in dry ice and kept cold during sample mounting. Diffraction data were collected between 230 and 330 K at the MS-powder beamline at the Swiss Light Source (SLS), PSI, Switzerland, using λ = 0.710162 Å and employing a MYTHEN detector.[12] Another experiment was performed between 100 and 340 K at the BM01 beamline at the European Synchrotron Radiation Facility (ESRF), France, using λ = 0.69449 Å and employing a Pilatus 2M area detector. Diffraction images obtained at BM01 were integrated by using the Bubble software.[13] The capillary was rotated during data acquisition. Data were subjected to Rietveld refinement using the program package FULLPROF.[14] The structural model from ref 8 was used for Rietveld refinements. The background was described by linear interpolation between selected points, while pseudo-Voigt profile functions were used to fit the diffraction pattern. The scale factor, unit cell parameters, zero shift, profile parameters (U, V, W), atomic displacement parameter (B), and the background were refined.

2.3. Neutron Scattering Investigations. The neutron experiments were performed at the ISIS Neutron and Muon Source in the UK by using the instruments OSIRIS and TOSCA.[15−18] The powdered $NH_4{}^{11}BH_4$ sample was evenly distributed in an aluminum pouch and packed into a flat plate cell for TOSCA and an annular double-walled sample cell for OSIRIS. The packing was done in an argon-filled glovebox while keeping both the sample and the sample cell cold with dry ice. The sample cells were cold-transferred to the neutron instruments, rapidly mounted on the sample sticks, and inserted into the instrument cryostats at 200 K. Subsequently, the samples were cooled to about 100 K. It has previously been reported that rapid cooling through the polymorphic transition at around 60 K can freeze NH_4BH_4 into a metastable polymorph.[6,7] To avoid this, the cooling rate in both experiments was kept below 2 K/min in the studied temperature region. The INS spectra were recorded in the temperature interval 10−100 K on TOSCA, whereas the quasi-elastic neutron scattering (QENS) spectra were recorded in the interval 10−240 K by using OSIRIS.

Elastic fixed-window scans (EFWS) were extracted from the QENS spectra collected upon heating from 10 to 240 K. In an EFWS experiment the intensity of a narrow energy slice centered at the elastic peak position is integrated for each individual temperature. When dynamics develops the integrated intensity decreases, since the quasi-elastic component becomes broader than the elastic peak (±25 μeV). The total scattering intensity (sum of elastic and quasi-elastic) is constant, and the quasi-elastic intensity (corresponding to reorientational dynamics) can therefore be estimated from the decrease of the elastic intensity.

2.4. Theoretical Calculations. A 2 × 2 × 2 supercell (SC) containing 320 atoms (Z = 32) was created from the conventional fcc unit cell with Z = 4 (UC). Density functional theory (DFT) calculations were performed using the Vienna Ab Initio Simulation Package (VASP[19,20]) in the framework of the frozen-core all-electron projector augmented wave method (PAW)[21,22] within the generalized gradient approximation (GGA) using the Perdew−Burke−Ernzerhof (PBE) exchange-correlation functional.[23,24] The cutoff energy for the plane waves was set to 520 eV. Structural relaxations were performed with total energies converged better than 1×10^{-4} eV. *Ab initio* MD calculations were performed using the SC in the NVT (constant number of atoms (N), volume (V), and temperature (T)) ensemble and employing a Nosé−Hoover thermostat at 300 K with the default Nosé mass parameter as set by VASP. The Brillouin zone integration was performed at the Γ-point. The integration time step was set to 1 fs. The total simulation time was about 5.3 ps after equilibration. All stresses were

DOI: 10.1021/acs.jpcc.9b08968
J. Phys. Chem. C 2019, 123, 28631−28639

converged at least within 4 kbar. For the 0 K structural relaxation of SCs only the Γ-point was used, whereas a denser 4 × 4 × 4 Monkhorst−Pack (MP) grid was applied to obtain total energies.[25] Z = 4 (40 atoms) cells were relaxed on a 4 × 4 × 4 MP grid, and the same mesh was used for total energy calculations. MD snapshots (referring to SCs with Z = 32) and UCs (Z = 4, extracted from the MD snapshots) were relaxed with all combinations of restricted/unrestricted N and B atom mobility (i.e., selective/nonselective dynamics, respectively, as implemented in VASP) and fixed cubic/unrestricted cell shape relaxation of the simulation box. Restricted N and B mobility implied the placement of the N and B atoms on the positions of the ideal NaCl structure where they were forced to remain during the simulations.

For extracting UCs from Z = 32 MD snapshots, first the positions on the ideal NaCl structure were assigned to the positions of the N and B atoms. Then their H ligands were identified and located so that bond directions and distances were kept as in the MD snapshot. UCs were extracted from 17 snapshots, after various times between 1.6 and 4.8 ps. The total number of VASP-relaxed UCs was 130. The phonon dispersions of several selected Z = 4 UCs were calculated based on the relaxed structures and using the small displacement method with 0.03 Å displacements as implemented in PhonoPy.[26] The total energy was converged better than 10^{-8} eV on a 4 × 4 × 4 MP grid and using a 520 eV plane wave energy cutoff.

The elastic constants were calculated for a simulation time-averaged MD structure using volume nonconserving distortions up to 10% in steps of 2%, according to the procedure described by Vekilova.[27] The calculations were performed on a Γ-centered k-mesh and using a 520 eV plane wave cutoff and a fixed cell shape. The influence of van der Waals (vdW) corrections was checked by using the DFT-D2 method by Grimme which is implemented in VASP.[28,29] These calculations were performed with the same cutoffs and k-point grids as for the noncorrected simulations.

3. RESULTS AND DISCUSSION

3.1. Energetics of Dihydrogen Bonding. Investigations into the crystal structure of NH_4BH_4 have been performed earlier using synchrotron powder X-ray diffraction at room temperature (on a slightly pressurized sample)[8] and powder neutron diffraction at 60 K and below.[6] From the room temperature synchrotron data Flacau et al. deduced a H disorder model where H atoms were placed at two 32f Wyckoff positions in the Fm-3m Z = 4 unit cell, with half-occupancies, each describing a cube-like distribution of H around B and N.[8] From the 60 K neutron data (of a deuterated sample) an essentially spherical distribution of D atoms around N was established, whereas the D arrangement around B was cube-like as in the model based on room temperature synchrotron data. Below 60 K transitions into a rhombohedral and a trigonal (or monoclinic) polymorph were reported.[6,7]

Figure 1a shows the Rietveld fit of our synchrotron data at room temperature. Our refinement essentially reproduced the earlier finding of Flacau et al.[8] The inclusion of H at the 32f positions (giving rise to the cube-like distribution) considerably improved the fit. However, it must be noted that reliable H disorder models can only be extracted from neutron diffraction data of deuterated samples. The cube-like distribution deduced from room temperature synchrotron data should be merely seen as a consequence of more or less

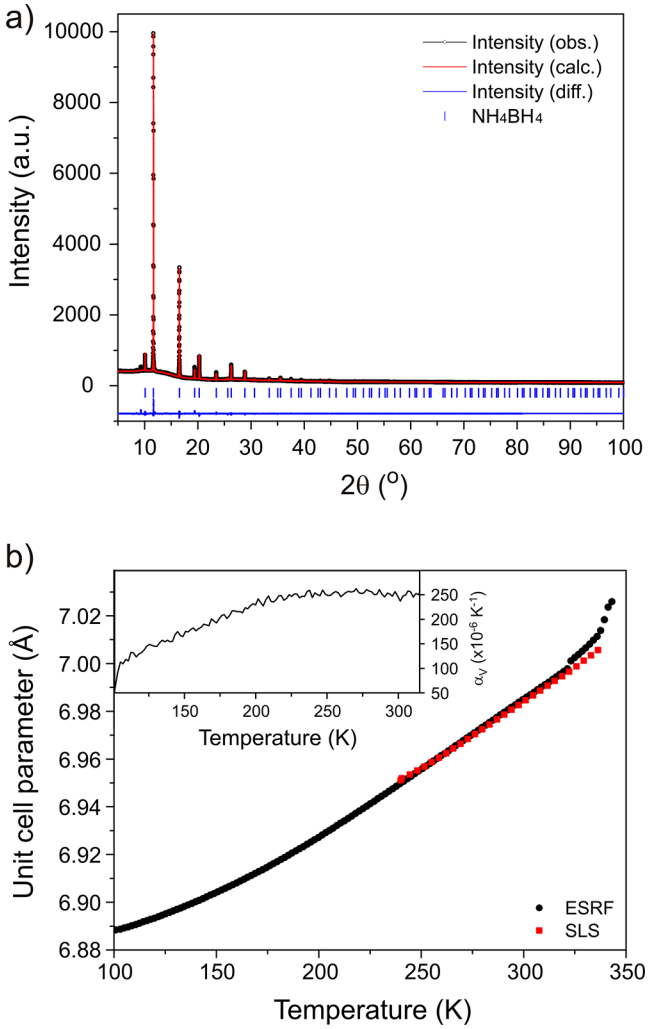

Figure 1. (a) Rietveld fit to SR PXD data of NH_4BH_4 measured at the SLS at T = 297 K (λ = 0.710162 Å), showing experimental (red circles) and calculated (black line) diffraction patterns, and a difference plot below (blue line). The employed structure model considered H disorder according to ref 8. The refined unit cell parameter is 6.98248(7) Å. Final discrepancy factors: R_p = 1.34%, R_{wp} = 1.76% (not corrected for background), R_p = 16.2%, R_{wp} = 14.9% (conventional Rietveld R-factors), R_{Bragg} = 4.20%, and global χ^2 = 3.43. (b) Lattice parameter of NH_4BH_4 extracted by sequential Rietveld refinement of SR PXRD data measured at the ESRF (λ = 0.69449 Å) in the temperature range T = 100−340 K (black symbols) and at the SLS (λ = 0.710162 Å) in the temperature range T = 230−330 K (red symbols). The inset shows the linear thermal expansion coefficient as a function of temperature in the temperature range T = 100−315 K.

randomly oriented tetrahedral ions. Figure 1b shows the evolution of the lattice parameter of NH_4BH_4 upon heating from 100 K up to the decomposition. Between 225 and 320 K the lattice parameter changes linearly. The corresponding volumetric thermal expansion coefficient is 250 × 10^{-6} K^{-1}, which is similar to BH_3NH_3 in the same temperature range[30] and rather compares to a liquid (e.g., water at 25 °C: 207 × 10^{-6} K^{-1}) than a soft ionic solid (e.g., CsI: 54 × 10^{-6} K^{-1}).[31]

Our computational investigation started with an *ab initio* MD simulation using a 2 × 2 × 2 supercell (Z = 32) at 300 K. The starting model corresponded to a NaCl structure of B and N atoms and using the experimental lattice parameter at 297 K,

DOI: 10.1021/acs.jpcc.9b08968
J. Phys. Chem. C 2019, 123, 28631−28639

a = 6.9825 Å (cf. Figure 1a). After equilibration at 300 K, the MD trajectories were collected for a period exceeding 5 ps. In agreement with previous studies, both NH_4^+ and BH_4^- moieties show high mobility.[8] For NH_4^+ this involves both, rotational diffusion around tetrahedral C_3 and C_2 axes and reorientational jumps of tetrahedra, whereas BH_4^- preferentially undergoes reorientational jumps. The snapshot shown in Figure 2a refers to 5 ps where complete equilibration can be

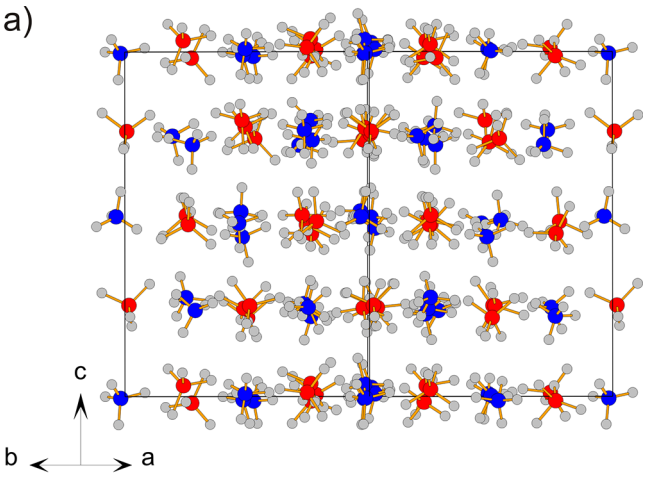

Figure 2. Z = 32 MD snapshot after 5 ps (a) and average positions of B and N atoms after 3 ps (b). N, B, and H atoms are shown in blue, red, and gray, respectively.

assumed. The average positions of B and N atoms clearly deviate from the high symmetry positions of the NaCl structure (Figure 2b).

To investigate the energetic consequences of the deviation of B and N atom positions from the ideal NaCl structure, we relaxed several Z = 32 MD snapshots with all combinations of restricted/unrestricted N and B atom mobility and cubic/unrestricted shape of the simulation box. These relaxations yielded essentially the same result with respect to total energy and equilibrium volume, irrespective of the Z = 32 starting configuration. Figure 3 shows a representative example. Forcing B and N atoms on the high symmetry positions of the NaCl structure leads to a slightly higher total energy, by about 4 meV per atom (3.9 kJ/mol). At the same time the equilibrium volume of the positionally restricted structure is

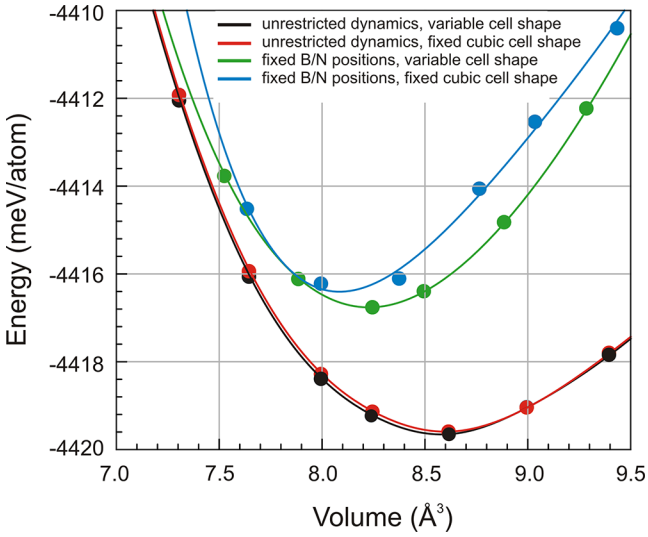

Figure 3. DFT relaxation of a Z = 32 snapshot obtained after 5 ps MD simulation time. Fixed B/N positions refer to selected dynamics where B and N atoms were forced on the positions of the NaCl structure. Variable shape refers to a relaxation algorithm with variable cell shape, whereas fixed cubic cell shape implies that the simulation cells had a constrained cubic shape.

smaller, 8.1−8.25 Å^3/atom, as compared to 8.5−8.6 Å^3/atom for the unrestricted structure. Interestingly, the former values are in good agreement with the experimental value at low temperatures (cf. Figure 1b)—to which the DFT relaxed structure is expected to relate more closely—whereas the latter appears considerably expanded. On the other hand, providing flexibility to the cell shape (i.e., allowing deviations from the cubic metric) does not add a significant stabilizing contribution. Figures 4a and 4b depict relaxed structures for the unrestricted and the enforced NaCl arrangement, respectively. One notices that BH_4^- ions adopt two preferred orientations, thus mimicking an average cubic environment. These cubes are aligned with their C_4 axes along ⟨100⟩ for the NaCl enforced arrangement, whereas they appear slightly distorted and tilted in the unrestricted structure. We note that there is a close correspondence to the disorder model refined from neutron diffraction data obtained at 60 K.[6] A possibly ordered structure arrangement, as indicated in experiments below 60 K, could not be identified from relaxed Z = 32 supercells.

We further calculated stresses vs distortions and the elastic constants of NH_4BH_4 based on the Z = 32 supercell, as described above. We obtained the following elastic constants: C_{11} = 12.4 GPa, C_{12} = 5.6 GPa, and C_{44} = 4.8 GPa. The mechanical stability of a cubic crystal requires $C_{44} > 0$, $C_{11} > 0$, $C_{11} + 2C_{12} > 0$, and $C_{11} - C_{12} > 0$. Thus, NH_4BH_4 described with a Z = 32 supercell is mechanically stable. The bulk modulus attains a very small value, B = 7.9 GPa, which mirrors the extreme softness of the material. In comparison, soft CsI has higher values for the bulk modulus and elastic constants (B = 12.7 GPa, C_{11} = 24.6 GPa, C_{12} = 6.7 GPa, and C_{44} = 6.2 GPa).[32] The ultimate test of the stability of the Z = 32 supercell would be a phonon dispersion calculation. However, such calculations were too expensive to perform. Yet we conjecture that Z = 32 supercells capture adequately the short and medium range interaction associated with dihydrogen bonding in NH_4BH_4.

DOI: 10.1021/acs.jpcc.9b08968
J. Phys. Chem. C 2019, 123, 28631−28639

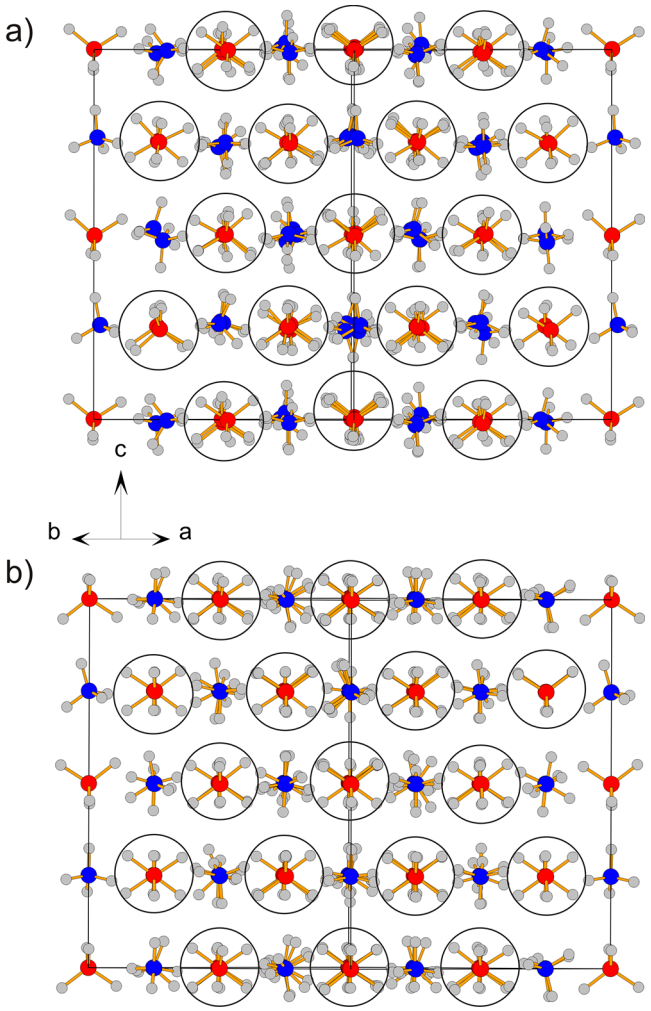

Figure 4. DFT relaxed structure of a $Z = 32$ MD snapshot after 5 ps. Unrestricted relaxation with variable cell shape (a) and only H atom relaxation with B and N atoms fixed on NaCl positions in a cubic simulation cell (b). The energy difference between the two configurations is about 3.5 meV/atom (cf. Figure 3). N, B, and H atoms are shown in blue, red, and gray, respectively. BH_4^- complexes are encircled to emphasize their two preferred orientations.

In the next step, cell sizes were reduced to $Z = 4$ (i.e., to the size of the conventional fcc unit cell). These $Z = 4$ cells were extracted from $Z = 32$ MD snapshots, as described above, and contained NH_4^+ and BH_4^- ions with different mutual orientations. Figure 5 shows the distribution of energies and equilibrium volumes of these configurations after (completely unrestricted) DFT relaxation. It is seen that the total energy differences are minute and close to the precision of the applied DFT method. The equilibrium volumes are scattered between 8.3 and 8.7 Å^3/atom, which is similar to the unrestricted relaxation of $Z = 32$ cells (cf. Figure 3). For each value of V (E_0) there are several values of E_0 (V) which can be viewed as the distribution of local minima provided by dihydrogen bonding. This implies that different relaxed configurations are essentially energetically degenerate, which is reminiscent of a glass. Clearly, dihydrogen bonding in NH_4BH_4 has no great tendency to induce long-range ordering. This is different for BH_3NH_3 which adopts a H-ordered structure with a small, $Z = 2$, unit cell below 220 K.[4,30]

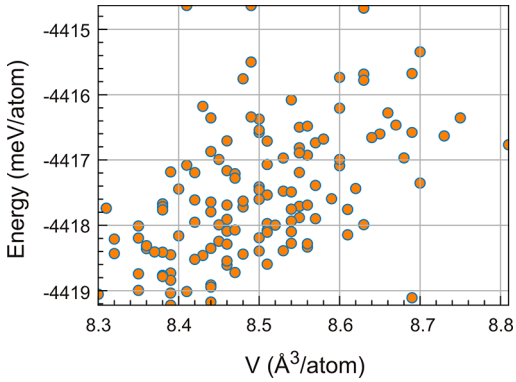

Figure 5. Distribution of equilibrium total energies and volumes of about 130 $Z = 4$ trial cells for NH_4BH_4.

Figure 6 compares the environments of a selection of complexes in $Z = 4$ cells after completely unrestricted DFT relaxation, giving an impression of the dihydrogen bonding pattern in NH_4BH_4. First, the feature of two preferred BH_4^- orientations as seen in $Z = 32$ supercells is reproduced in the $Z = 4$ cells. An interesting observation is that, nevertheless, there is a greater variability of dihydrogen contacts from hydridic H (attached to BH_4^- to protonic H (attached to NH_4^+) than vice versa. Dihydrogen contacts are considered for a distance range from 1.7 to 2.3 Å (i.e., below the sum of the van der Waals radii for two hydrogen atoms, 2.4 Å),[4] and in all investigated SCs and UCs there is a pronounced minimum in the distribution of $H^{\delta+}$−$H^{\delta-}$ distances between 2.3 and 2.6 Å. A hydridic H attached to B can be connected to 1, 2, or 3 protonic H attached to a neighboring N. There is some preference for 2-fold contacts, but 1- and 3-fold contacts are common and occur with a similar frequency. In contrast the great majority (80−90%) of protonic H attached to N is connected to two hydridic H and one- and 3-fold contacts are rare. In addition, two-contact dihydrogen bonding of the protonic H displays a rather rigid geometry where the triangle of H atoms and the N−H bond are close to coplanar. We note that results with and without vdW corrections were very similar with respect to equilibrium volumes and structures of $Z = 4$ cells.

The V−E_0 relations obtained for $Z = 4$ cells are very close to the ones obtained for the $Z = 32$ supercells. Thus, it appears that also $Z = 4$ cells describe properly the energetics of dihydrogen bonding in NH_4BH_4, which in turn has to be assumed more or less nondirectional. However, it is important to note that $Z = 4$ cells do not appear dynamically stable. Phonon dispersions were calculated for a range of cells with lowest E_0 and for all imaginary branches obtained (also when including vdW corrections). These imaginary branches could be associated with libration modes. Therefore, $Z = 4$ cells may not account adequately for the short- and medium-range interaction of dihydrogen bonding. Next, we investigate how dihydrogen bonding in NH_4BH_4 expresses in vibrational spectroscopy.

3.2. Vibrational Properties of NH_4BH_4. *3.2.1. Raman Spectroscopy: Internal Modes.* The two tetrahedral ions NH_4^+ and BH_4^- constituting NH_4BH_4 will each give rise to 9 internal modes, 4 stretches (A_1 + F_2), and 5 bends (E + F_2). All stretches and bends (four bands in total) are observable with Raman spectroscopy. They are denoted as $\nu_1(A_1)$ (symmetric stretching mode), $\nu_3(F_2)$ (asymmetric stretching mode), ν_2(E)

DOI: 10.1021/acs.jpcc.9b08968
J. Phys. Chem. C 2019, 123, 28631−28639

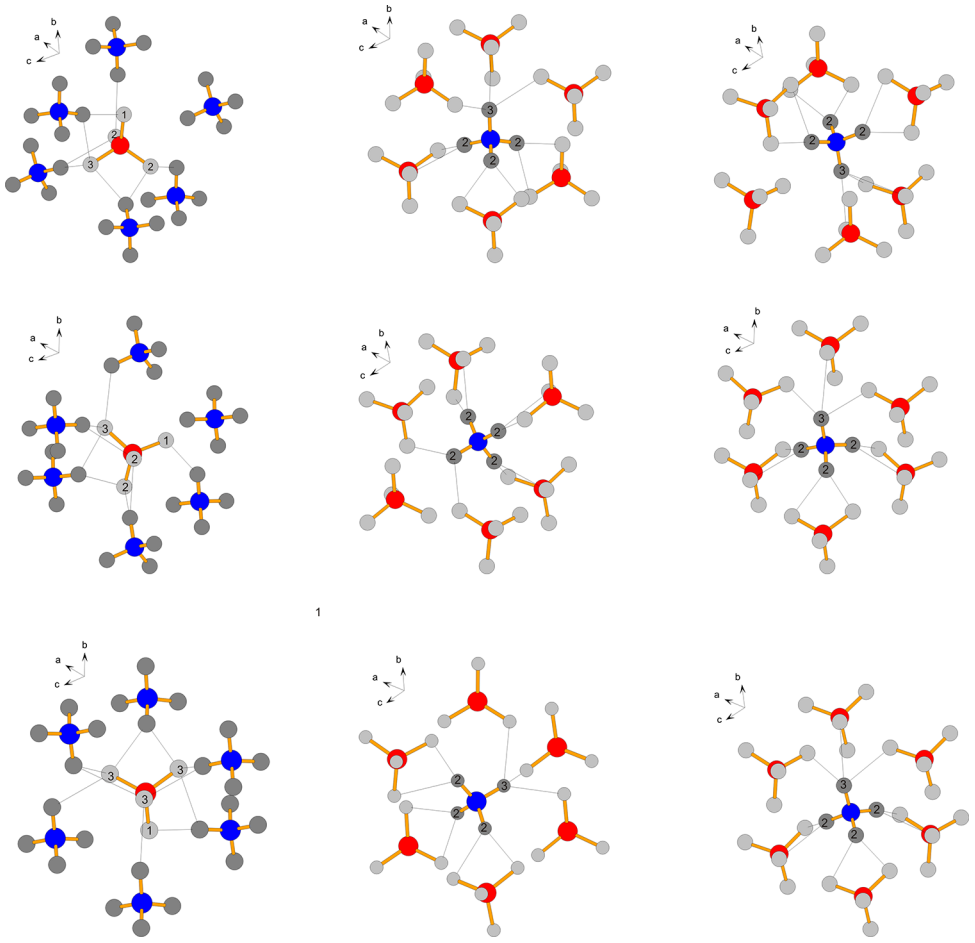

Figure 6. Dihydrogen-bonding environment of a selection of BH_4^- (left) and NH_4^+ complexes (right) as extracted from fully DFT relaxed $Z = 4$ NH_4BH_4 cells. N and B atoms are shown in blue and red, respectively. Protonic and hydridic hydrogen atoms are shown dark and light gray, respectively. The projection is roughly along ⟨111⟩ with respect to a cubic cell. Note that BH_4^-complexes attain two preferred orientations, up and down. Dihydrogen bonds (below 2.3 Å) are drawn as thin lines. The numbers indicate the number of contacts.

(symmetric bending mode), and $\nu_4(F_2)$ (asymmetric bending mode). In the solid there are in addition external (lattice) modes: Each ion will give rise to three libration (torsion) modes (i.e., six in total), and there are three translation modes where the center of mass of the complexes represents the main displacements. Libration and translation modes are forbidden in Raman spectra for the fcc NaCl structure.

Figure 7 shows the Raman spectrum for NH_4BH_4 at 98 K as reported by Karkamkar et al.[3] for which we assigned the modes. The bands from BH_4^- and NH_4^+ are well-separated. The modes for BH_4^- are strikingly similar to those of $RbBH_4$, which adopts the H disordered fcc structure above 20 K.[33] For $RbBH_4$, B−H bond bending vibrations occur at about half the stretching vibrations, which cause overtones and Fermi resonance. B−H bends are at 1107 and 1237 cm^{-1}. Accordingly, the bands at 2159 and 2197 cm^{-1} represent the overtone of the asymmetric bend, which is split because of Fermi resonance with A_1 and F_2 stretches. B−H stretches are at ∼2280 cm^{-1} (asymmetric) and 2295 cm^{-1} (symmetric). The modes for NH_4^+ compare very well to NH_4I, which attains the disordered fcc structure above 256 K.[34] For fcc NH_4I the stretches ν_1 and ν_3 are at 3075 and 3127 cm^{-1}, respectively, and the bends ν_2 and ν_4 are at 1632 and 1410 cm^{-1}, respectively.[34,35] For NH_4BH_4, the N−H stretches are observed at 3118 and 3178 cm^{-1}. Of the two N−H bends only one (ν_4 at 1404 cm^{-1}) is clearly visible. The symmetric

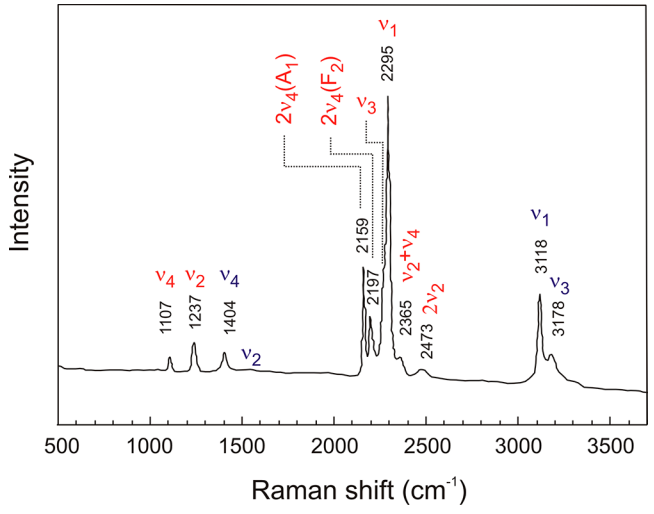

Figure 7. Raman spectrum of NH_4BH_4 taken at 98 K according to Karkamkar et al.[3] Modes stemming from BH_4^- and NH_4^+ are labeled in red and blue, respectively.

bend ν_2 is expected at around 1650 cm^{-1}. In conclusion, the Raman spectrum of NH_4BH_4 at 98 K can be interpreted as a superposition of the spectra of fcc $RbBH_4$ and NH_4I. Thus, peculiarities due to dihydrogen bonding are not apparent for

DOI: 10.1021/acs.jpcc.9b08968
J. Phys. Chem. C 2019, 123, 28631−28639

the internal modes. Possibly such peculiarities reveal in the external modes (i.e., librations and translations) which can be analyzed by INS spectroscopy.

According to earlier NMR studies,[8] both NH_4^+ and BH_4^- moieties are dynamically disordered down to 77 K. At the same time, previous neutron diffraction investigations at low temperatures showed that NH_4BH_4 undergoes structural transitions when cooling below 60 K. To assist the INS study, it was deemed necessary to obtain more information into these transitions and also the overall dynamical behavior of NH_4^+ and BH_4^- ions. For this, we performed an EFWS for NH_4BH_4 in the temperature range 10−240 K and normalized the data to the data point at the lowest temperature. As shown in Figure 8, EFWS is a useful indicator of the *T*-dependent

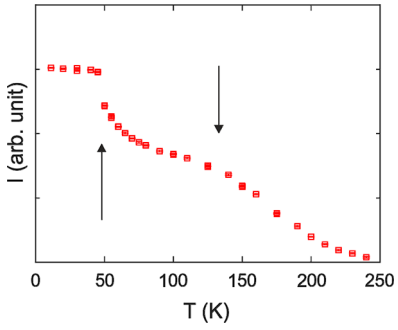

Figure 8. Neutron elastic-fixed-window scan for NH_4BH_4 upon heating from 4 to 240 K. Arrows indicate changes in the dynamical behavior. The first (at 50 K) is attributed to the transition from the dynamically ordered low temperature polymorph to the fcc polymorph with mobile NH_4^+ ions and the second to the onset of BH_4^- dynamics (with jump frequencies faster than $\approx 10^{-9}$ s).

dynamical behavior of the H atoms. The virtually *T*-independent behavior below 50 K shows the absence of any active dynamical processes. At 50 K a drop occurs in the elastic intensity which signals the onset of H dynamics. This intensity decrease then levels off until 125 K, after which a change in slope gives evidence of a second dynamical process. Thus, the EFWS suggests a dynamically frozen state below 50 K, a structural transition at around 50 K, which is associated with H atom (reorientational) mobility, and a change in the dynamical behavior above 125 K. The observed structural transition should be to the fcc phase which, thus, occurs at a somewhat lower temperature than reported earlier.[6,7]

3.2.2. INS Spectroscopy: External Modes. The INS spectra are shown in Figure 9. Measurements were performed upon heating from base temperature 5 K. Internal modes are above 1000 cm^{-1}, in agreement with the Raman spectrum, and external modes are below 400 cm^{-1} (Figure 9a). Generally, the spectral intensity is strongly suppressed above 1500 cm^{-1} because of the Debye−Waller factor.[10] That is stretching modes (above 2000 cm^{-1}) are barely discernible from the background in the TOSCA spectrum (Figure 9b).[11] The location of bending modes is in very good agreement with the Raman spectrum (cf. Figure 8). As a matter of fact, the bending mode region in the 100 K INS spectrum and 98 K Raman spectrum are virtually identical. The structural transition seen in the EFWS is also clearly revealed in the INS spectra in the temperature range 46−49 K: There is a large increase in scatter intensity close to the elastic line due to QENS, which signifies transition to a dynamically disordered phase (Figure 9a). Upon cooling the phase transition occurs

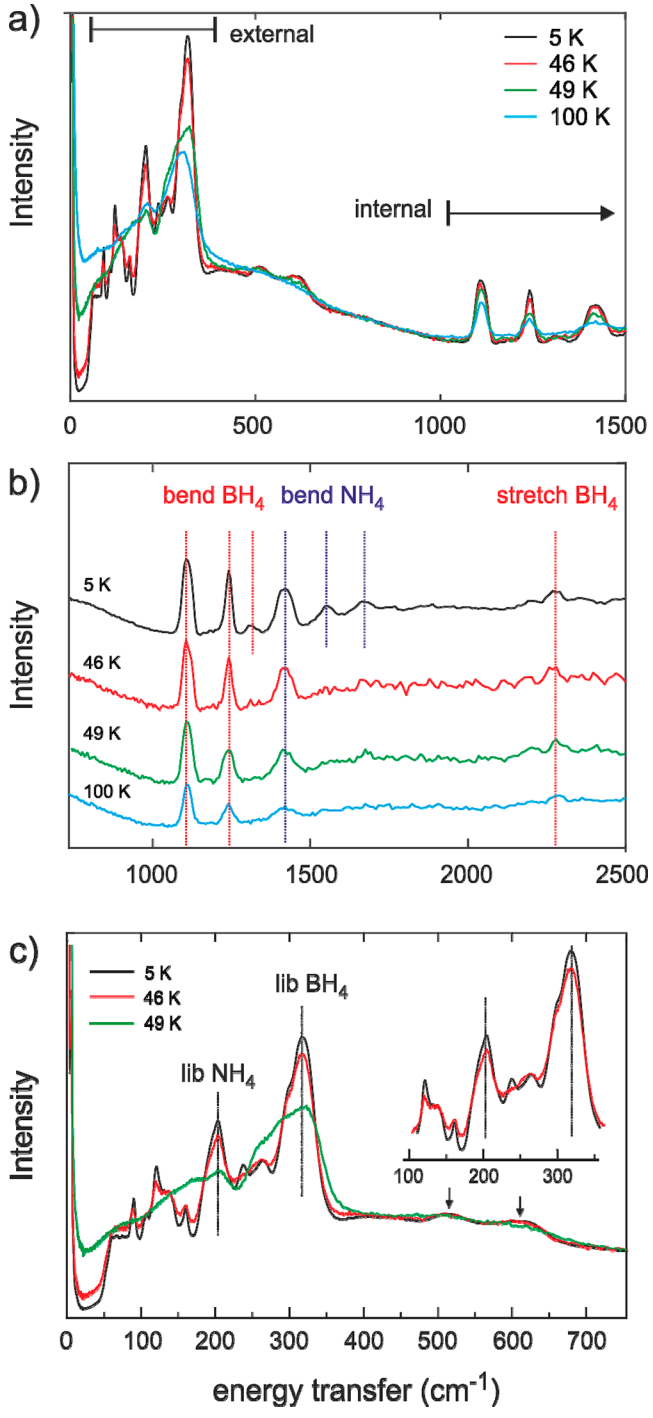

Figure 9. INS spectra of NH_4BH_4 at selected temperatures during heating from base temperature 5 to 100 K. (a) Spectral range from 0 to 1500 cm^{-1} showing the division of internal and external modes. (b) External modes up to 2500 cm^{-1}. (c) Evolution of internal modes. The arrows mark intensity attributed to overtones/combinations of BH_4^- and NH_4^+ librations. Vertical lines mark the location of BH_4^- and NH_4^+ librations.

between 45 and 40 K, which indicates a hysteresis of about 5 K.

Figure 9c shows the evolution of external modes with temperature. The spectrum at 5 K shows distinct and sharp bands below 200 cm^{-1} which are assigned to translation modes of the dynamically frozen low temperature phase. These bands are slightly changed in the 46 K spectrum, just below the

DOI: 10.1021/acs.jpcc.9b08968
J. Phys. Chem. C 2019, 123, 28631−28639

transition to the dynamically disordered fcc phase, which indicates the existence of a second dynamically frozen low-temperature phase (inset in Figure 9c). This is corroborated in the external modes (cf. Figure 9b) which show an additional BH_4^- bending mode in the 5 K spectrum (in addition to the bands corresponding to ν_2 and ν_4 in the Raman spectrum), which suggests a lower symmetry structure at 5 K. The broad bands at around 300 and 200 cm^{-1} are assigned to the libration modes of BH_4^- and NH_4^+, respectively. An additional (weak) intensity at about 500 and 650 cm^{-1} is attributed to the combination of NH_4^+ and BH_4^- libration and the BH_4^- libration overtone, respectively. The transition to the dynamically disordered fcc phase manifests itself with the disappearance of the translation modes and the libration modes of NH_4^+.

Unlike the NH_4^+ libration modes, the band associated with BH_4^- librations is still well recognizable after the structural transition, although it loses intensity. The abrupt increase in width and more asymmetric shape indicate considerable changes in the potential energy surface along the torsional coordinate. Again, there is a strong resemblance to the heavier alkali metal borohydrides, $NaBH_4$–$CsBH_4$. At 4 K the BH_4^- libration band for these compounds has its peak between 300 cm^{-1} (Cs) and 355 cm^{-1} (Na)[36,37] which is very similar to NH_4BH_4. As shown by Verdal et al., the libration band is considerably broadened but maintained after the order–disorder transition into the fcc phase, which occurs at temperatures between 25 K (Cs) and 190 K (Na).[37] At the same time Udovic et al. demonstrated the presence of (comparatively slow) torsional motion on the order of 10^8–10^9 jumps/s in the alkali metal borohydride fcc phases at temperatures where a libration band is still present.[38]

A detailed analysis of NH_4^+ and BH_4^- dynamics in NH_4BH_4 will be the subject of a forthcoming QENS study. However, from the evolution of the INS spectra and the EFWS it can be inferred that the mobility of the two kinds of complex ions is very different. Whereas NH_4^+ undergoes fast reorientational dynamics already at the onset of the transition to the fcc phase, BH_4^- dynamics appears to be much more hindered. The more slowly moving BH_4^- would distribute with two orientations and giving the impression of an average cubic environment, as seen in the crystallographic disorder model refined from neutron diffraction data at 60 K[6] and also established from the DFT relaxations in this work. This is the case for temperatures below 100 K. Above 100 K the EFWS indicates then significant BH_4^- dynamics.

Lastly we comment on the libration band of NH_4^+ which is seen at around 200 cm^{-1} in the dynamically frozen state below 50 K. The location of NH_4^+ libration bands expresses the strength of the interaction with the anion environment. Within the halide series, it is above 500 cm^{-1} for NH_4F[39] and down to 270–280 cm^{-1} for NH_4I.[40,41] Compared to this series, the libration band of NH_4^+ in NH_4BH_4 is at very low wavenumbers which indicates that dihydrogen bonding implies a soft torsional potential for NH_4^+, whereas the one for BH_4^- is very similar to a alkali metal environment.

4. CONCLUSION

Ammonium borohydride, being composed of the tetrahedral complex ions NH_4^+ and BH_4^-, possesses one of the highest H density among solid compounds. The simultaneous presence of B-hydridic and N-protonic H gives rise to intermolecular dihydrogen bonding which is considered peculiar in NH_4BH_4 because of the large number of possible $H^{\delta+}$–$H^{\delta-}$ contacts. In the high-temperature form, complexes are arranged as in the fcc NaCl structure. Upon cooling, INS spectra revealed a structural transition between 45 and 40 K. This transition is reversible and occurs upon heating between 46 and 49 K. The different behavior of librational modes for NH_4^+ and BH_4^- suggests that, upon entering the fcc high-temperature form, NH_4^+ ions attain fast reorientational dynamics whereas BH_4^- ions become significantly mobile only at temperatures above 100 K. The vibrational behavior of BH_4^- ions in NH_4BH_4 compares well to the heavier alkali metal borohydrides $NaBH_4$–$CsBH_4$ in which BH_4^- ions adopt two preferred orientations which mimic an average cube-like distribution of H atoms around B. DFT simulations using $Z = 32$ and $Z = 4$ cells revealed a nondirectional nature of dihydrogen bonding in NH_4BH_4, with only weak tendency for long-range order. Relaxed structures with different rotational configurations of complex ions appeared energetically quasi-degenerate which is reminiscent of a glassy state.

AUTHOR INFORMATION

Corresponding Author

*E-mail: Ulrich.Haussermann@mmk.su.se.

ORCID

Jakob B. Grinderslev: 0000-0001-7645-1383
Jeff Armstrong: 0000-0002-8326-3097
Maths Karlsson: 0000-0002-2914-6332
Ulrich Häussermann: 0000-0003-2001-4410

Notes

The authors declare no competing financial interest.

ACKNOWLEDGMENTS

This work was supported by Nordforsk within the project FunHy. M.S.A. acknowledges support from the Swedish research council (VR). S.F. acknowledges the financial support from Carl Tryggers Stiftelse (CTS) för Vetenskaplig Forskning. The computations were performed on resources provided by the Swedish National Infrastructure for Computing (SNIC) at High Performance Computing Center North (HPC2N). Experiments at the ISIS Neutron and Muon Source were supported by beamtime allocations from the Science and Technology Facilities Council. S.F. and S.I.S. acknowledge Åke Sandgren at HPC2N for excellent and fast support of this work. Support from the Swedish Government Strategic Research Area in Materials Science on Advanced Functional Materials at Linköping University (Faculty Grant SFO-Mat-LiU No. 2009-00971) is acknowledged by S.I.S.

REFERENCES

(1) Nielsen, T. K.; Karkamkar, A.; Bowden, M.; Besenbacher, F.; Jensen, T. T.; Autrey, T. Methods to stabilize and destabilize ammonium borohydride. *Dalton Trans* **2013**, *42*, 680–687.

(2) Parry, R. W.; Schultz, D. R.; Girardot, P. R. The preparation and properties of hexamminecobalt(III) borohydride, hexamminechromium(III) borohydride and ammonium borohydride. *J. Am. Chem. Soc.* **1958**, *80*, 1–3.

(3) Karkamkar, A.; Kathmann, S. M.; Schenter, G. K.; Heldebrant, D. J.; Hess, N.; Gutowski, M.; Autrey, T. Thermodynamic and structural investigations of ammonium borohydride, a solid with a highest content of thermodynamically and kinetically accessible hydrogen. *Chem. Mater.* **2009**, *21*, 4356–4358.

(4) Klooster, W. T.; Koetzle, T. F.; Siegbahn, P. E. M.; Richardson, T. B.; Crabtree, R. H. Study of the N – H··· H – B dihydrogen bond

DOI: 10.1021/acs.jpcc.9b08968
J. Phys. Chem. C 2019, 123, 28631–28639

including the crystal structure of BH_3NH_3 by neutron diffraction. *J. Am. Chem. Soc.* **1999**, *121*, 6337−6343.
(5) Custelcean, R.; Jackson, J. E. Dihydrogen bonding: structures, energetics, and dynamics. *Chem. Rev.* **2001**, *101*, 1963−1980.
(6) Ryan, K. R. A study of ammonia borane and its derivatives. Doctoral dissertation, University of Oxford, Oxford, UK, 2011.
(7) Hore, K. Ammonia borane and its derivatives: high weight percentage hydrogen storage materials. Doctoral dissertation, University of Oxford, Oxford, UK, 2013.
(8) Flacau, R.; Ratcliffe, C. I.; Desgreniers, S.; Yao, Y.; Klug, D. D.; Pallister, P.; Moudrakovski, I. L.; Ripmeester, J. A. Structure and dynamics of ammonium borohydride. *Chem. Commun.* **2010**, *46*, 9164−9166.
(9) Flacau, R.; Yao, Y.; Klug, D. D.; Desgreniers, S.; Ratcliffe, C. I. Structural phase transitions induced by pressure in ammonium borohydride. *Phys. Chem. Chem. Phys.* **2012**, *14*, 7005−7011.
(10) Mitchell, P. C. H.; Parker, S. F.; Ramirez-Cuesta, A. J.; Tomkinson, J. *Vibrational Spectroscopy with Neutrons, with Applications in Chemistry, Biology, Materials Science and Catalysis*; World Scientific: Singapore, 2005.
(11) Richter, B.; Grinderslev, J. B.; Møller, K. T.; Paskevicius, M.; Jensen, T. R. From metal hydrides to metal borohydrides. *Inorg. Chem.* **2018**, *57*, 10768−10780.
(12) Willmott, P. R.; Meister, D.; Leake, S. J.; Lange, M.; Bergamaschi, A.; Böge, M.; Calvi, M.; Cancellieri, C.; Casati, N.; Cervellino, A.; et al. The materials science beamline upgrade at the Swiss Light Source. *J. Synchrotron Radiat.* **2013**, *20*, 667−682.
(13) Dyadkin, V.; Pattison, P.; Dmitriev, V.; Chernyshov, D. A new multipurpose diffractometer PILATUS@SNBL. *J. Synchrotron Radiat.* **2016**, *23*, 825−829.
(14) Rodríguez-Carvajal, J. FULLPROF: A program for Rietveld refinement and pattern matching analysis. *Abstracts of the Satellite Meeting on Powder Diffraction of the XV IUCr Congress* **1990**, 127.
(15) Experiment RB1820371; STFC ISIS Facility, 2018.
(16) Experiment RB1810245; STFC ISIS Facility, 2018.
(17) Parker, S. F.; Fernandez-Alonso, F.; Ramirez-Cuesta, A. J.; Tomkinson, J.; Rudic, S.; Pinna, R. S.; Gorini, G.; Fernandez Castanon, J. Recent and future developments on TOSCA at ISIS. *J. Phys.: Conf. Ser.* **2014**, *554*, 012003.
(18) Pinna, R. S.; Rudić, S.; Parker, S. F.; Armstrong, J.; Zanetti, M.; Škoro, G.; Waller, S. P.; Zacek, D.; Smith, C. A.; Capstick, M. J.; et al. The neutron guide upgrade of the TOSCA spectrometer. *Nucl. Instrum. Methods Phys. Res., Sect. A* **2018**, *896*, 68−74.
(19) Kresse, G.; Hafner, J. Ab initio molecular dynamics for liquid metals. *Phys. Rev. B: Condens. Matter Mater. Phys.* **1993**, *47*, 558−561.
(20) Kresse, G.; Furthmüller, J. Efficient iterative schemes for ab initio total-energy calculations using a plane-wave basis set. *Phys. Rev. B: Condens. Matter Mater. Phys.* **1996**, *54*, 11169−11186.
(21) Blöchl, P. E. Projector augmented-wave method. *Phys. Rev. B: Condens. Matter Mater. Phys.* **1994**, *50*, 17953−17979.
(22) Kresse, G.; Joubert, D. From ultrasoft pseudopotentials to the projector augmented-wave method. *Phys. Rev. B: Condens. Matter Mater. Phys.* **1999**, *59*, 1758−1775.
(23) Perdew, J. P.; Burke, K.; Ernzerhof, M. Generalized gradient approximation made simple. *Phys. Rev. Lett.* **1996**, *77*, 3865−3868.
(24) Perdew, J. P.; Burke, K.; Ernzerhof, M. Generalized gradient approximation made simple- ERRATA. *Phys. Rev. Lett.* **1997**, *78*, 1396.
(25) Pack, J. D.; Monkhorst, H. J. Special points for Brillouin-zone integrations. *Phys. Rev. B* **1976**, *13*, 5188−5192.
(26) Togo, A.; Tanaka, I. First principles phonon calculations in materials science. *Scr. Mater.* **2015**, *108*, 1−5.
(27) Vekilova, O. Yu. Influence of stress and impurities on thermodynamics and elastic properties of metals and alloys from ab initio theory. Linköping Studies in Science and Technology. Dissertation No. 1531, 2013.
(28) Klimes, J.; Bowler, D. R.; Michaelides, A. Chemical accuracy for the van der Waals density functional. *J. Phys.: Condens. Matter* **2010**, *22*, 022201.
(29) Klimes, J.; Bowler, D. R.; Michaelides, A. Van der Waals density functionals applied to solids. *Phys. Rev. B: Condens. Matter Mater. Phys.* **2011**, *83*, 195131.
(30) Hess, N. J.; Schenter, G. K.; Hartman, M. R.; Daemen, L. L.; Proffen, T.; Kathmann, S. M.; Mundy, C. J.; Hartl, M.; Heldebrant, D. J.; Stowe, A. C.; Autrey, T. Neutron powder diffraction and molecular simulation study of the structural evolution of ammonia borane from 15 to 340 K. *J. Phys. Chem. A* **2009**, *113*, 5723−5735.
(31) Bailey, A. C.; Yates, B. The low temperature thermal expansion and related thermodynamic properties of alkali halides with a cesium chloride structure. *Philos. Mag.* **1967**, *16*, 1241−1248.
(32) Ribeiro, R. M.; Coutinho, J.; Torres, V. J. B.; Jones, R.; Sque, S. J.; Oberg, S.; Shaw, M. J.; Briddon, P. R. Ab initio study of CsI and its surface. *Phys. Rev. B: Condens. Matter Mater. Phys.* **2006**, *74*, 035430.
(33) Renaudin, G.; Gomes, S.; Hagemann, H.; Keller, L.; Yvon, K. Structural and spectroscopic studies on the alkali borohydrides MBH_4 (M = Na, K, Rb, Cs). *J. Alloys Compd.* **2004**, *375*, 98−106.
(34) Durig, J. R.; Antion, D. J. Low-frequency vibrations in ammonium iodide and ammonium bromide. *J. Chem. Phys.* **1969**, *51*, 3639−3647.
(35) Couture-Mathieu, L.; Mathieu, J. P. Spectres de vibration de sels d'ammonium cristallises. *J. Chim. Phys. Phys.-Chim. Biol.* **1952**, *49*, 226−237.
(36) Verdal, N.; Hartman, M. R.; Jenkins, T.; DeVries, D. J.; Rush, J. J.; Udovic, T. J. Reorientational dynamics of $NaBH_4$ and KBH_4. *J. Phys. Chem. C* **2010**, *114*, 10027−10033.
(37) Verdal, N.; Udovic, T. J.; Zhou, W.; Rush, J. J.; DeVries, D. J.; Hartman, M. R. Vibrational spectroscopic study of subtle phase transitions in alkali borohydrides: comparison with first-principles calculations. *J. Phys. Chem. C* **2013**, *117*, 876−883.
(38) Udovic, T. J.; Verdal, N.; Rush, J. J.; DeVries, D. J.; Hartman, M. R.; Vajo, J. J.; Gross, A. F.; Skripov, A. V. Mapping trends in the reorientational mobilities of tetrahydroborate anions via neutron-scattering fixed-window scans. *J. Alloys Compd.* **2013**, *580*, S47−S50.
(39) Adams, M. A.; Refson, K.; Gabrys, B. J. The high resolution inelastic neutron scattering spectrum of ammonium fluoride. *Phys. Chem. Chem. Phys.* **2005**, *7*, 3685−3692.
(40) Venkataraman, G.; Usha Deniz, K.; Iyengar, P. K.; Roy, A. P.; Vijayaraghavan, P. R. Study of the rotational behavior of the ammonium ion in several salts by neutron spectrometry. *J. Phys. Chem. Solids* **1966**, *27*, 1103−1123.
(41) Kavruk, D.; Yurtseven, H. Calculation of the Raman frequencies as a function of temperature in phase III of NH_4I. *Mod. Phys. Lett. B* **2010**, *24*, 817−824.

DOI: 10.1021/acs.jpcc.9b08968
J. Phys. Chem. C 2019, 123, 28631−28639